Isolated Bidirectional Full-Bridge DC–DC Converter With a Flyback Snubber

Tsai-Fu Wu, *Senior Member, IEEE*, Yung-Chu Chen, Jeng-Gung Yang, and Chia-Ling Kuo

***Abstract*—An isolated bidirectional full-bridge dc–dc converter with high conversion ratio, high output power, and soft start-up capability is proposed in this paper. The use of a capacitor, a diode, and a flyback converter can clamp the voltage spike caused by the current difference between the current-fed inductor and leakage inductance of the isolation transformer, and can reduce the current flowing through the active switches at the current-fed side. Operational principle of the proposed converter is first described, and then, the design equation is derived. A 1.5-kW prototype with low-side voltage of 48 V and high-side voltage of 360 V has been implemented, from which experimental results have verified its feasibility.**

***Index Terms*—Flyback converter, isolated full-bridge bidirectional converter, soft start-up.**

I. Introduction

IN RENEWABLE dc-supply systems, batteries are usually required to back-up power for electronic equipment. Their voltage levels are typically much lower than the dc-bus voltage. Bidirectional converters for charging/discharging the batteries are therefore required. For high-power applications, bridge-type bidirectional converters have become an important research topic over the past decade [1]–[7]. For raising power level, a dual full-bridge configuration is usually adopted [8]–[16], and its low side and high side are typically configured with boost-type and buck-type topologies, respectively. The major concerns of these studies include reducing switching loss, reducing voltage and current stresses, and reducing conduction loss due to circulation current. A more severe issue is due to leakage inductance of the isolation transformer, which will result in high voltage spike during switching transition. Additionally, the current freewheeling due to the leakage inductance will increase conduction loss and reduce effective duty cycle. An alternative approach [9] is to precharge the leakage inductance to raise its current level up to that of the current-fed inductor, which can reduce their current difference and, in turn, reduce voltage spike. However, since the current level varies with load condition, it is hard to tune the switching timing diagram to match these two currents. Thus, a passive or an active clamp circuit is still needed.

Manuscript received October 14, 2009; revised January 29, 2010; accepted February 10, 2010. Date of current version June 18, 2010. Recommended for publication by Associate Editor K. Ngo.

The authors are with the Elegant Power Application Research Center, Department of Electrical Engineering, National Chung Cheng University, Min-Hsiung 621, Taiwan (e-mail: ieetfwu@ccu.edu.tw).

Color versions of one or more of the figures in this paper are available online at http://ieeexplore.ieee.org.

Digital Object Identifier 10.1109/TPEL.2010.2043542

An active commutation principle was published [9] to control the current of leakage inductance; however, clamping circuits are additionally required. Passive and active clamping circuits have been proposed to suppress the voltage spikes due to the current difference between the current-fed inductor and leakage inductance of the isolation transformer [10], [14]. The simplest approach is employing an *RCD* passive snubber to clamp the voltage, and the energy absorbed in the clamping capacitor is dissipated on the resistor, thus resulting in lower efficiency. A buck converter was employed to replace an *RCD* passive snubber, but it still needs complex clamping circuits [17], [18]. A simple active clamping circuit was proposed [12], [19], which suits for bidirectional converters. However, its resonant current increases the current stress on switches significantly. In [20], Wang *et al.* proposed a topology to achieve soft-starting capability, but it is not suitable for step-down operation.

This paper introduces a flyback snubber to recycle the absorbed energy in the clamping capacitor. The flyback snubber can be operated independently to regulate the voltage of the clamping capacitor; therefore, it can clamp the voltage to a desired level just slightly higher than the voltage across the low-side transformer winding. Since the current does not circulate through the full-bridge switches, their current stresses can be reduced dramatically under heavy-load condition, thus improving system reliability significantly. Additionally, during start-up, the flyback snubber can be controlled to precharge the high-side capacitor, improving feasibility significantly. A bidirectional converter with low-side voltage of 48 V, high-side voltage of 360 V, and power rating of 1.5 kW has been designed and implemented, from which experimental results have verified the discussed performance.

II. Configuration and Operation

The proposed isolated bidirectional full-bridge dc–dc converter with a flyback snubber is shown in Fig. 1. The converter is operated with two modes: buck mode and boost mode. Fig. 1 consists of a current-fed switch bridge, a flyback snubber at the low-voltage side, and a voltage-fed bridge at the high-voltage side. Inductor L_m performs output filtering when power flows from the high-voltage side to the batteries, which is denoted as a buck mode. On the other hand, it works in boost mode when power is transferred from the batteries to the high-voltage side. Furthermore, clamp branch capacitor C_C and diode D_C are used to absorb the current difference between current-fed inductor L_m and leakage inductance L_{ll} and L_{lh} of isolation transformer T_x during switching commutation.

The flyback snubber can be independently controlled to regulate V_C to the desired value, which is just slightly higher than

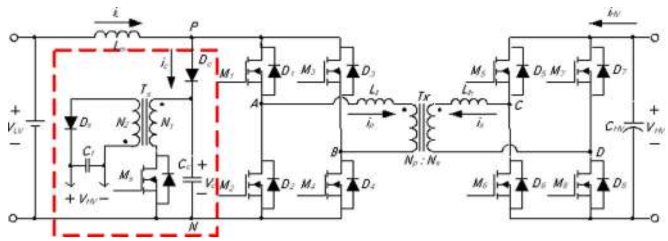

Fig. 1. Isolated bidirectional full-bridge dc–dc converter with a flyback snubber.

V_{AB}. Thus, the voltage stress of switches M_1–M_4 can be limited to a low level. The major merits of the proposed converter configuration include no spike current circulating through the power switches and clamping the voltage across switches M_1–M_4, improving system reliability significantly. Note that high spike current can result in charge migration, over current density, and extra magnetic force, which will deteriorate in MOSFET carrier density, channel width, and wire bonding and, in turn, increase its conduction resistance.

A bidirectional dc–dc converter has two types of conversions: step-up conversion (boost mode) and step-down conversion (buck mode). In boost mode, switches M_1–M_4 are controlled, and the body diodes of switches M_5–M_8 are used as a rectifier. In buck mode, switches M_5–M_8 are controlled, and the body diodes of switches M_1–M_4 operate as a rectifier. To simplify the steady-state analysis, several assumptions are made, which are as follows.

1) All components are ideal. The transformer is treated as an ideal transformer associated with leakage inductance.
2) Inductor L_m is large enough to keep current i_L constant over a switching period.
3) Clamping capacitor C_C is much larger than parasitic capacitance of switches M_1–M_8.

A. Step-Up Conversion

In boost mode, switches M_1–M_4 are operated like a boost converter, where switch pairs (M_1, M_2) and (M_3, M_4) are turned ON to store energy in L_m. At the high-voltage side, the body diodes of switches M_5–M_8 will conduct to transfer power to V_{HV}. When switch pair (M_1, M_2) or (M_3, M_4) is switched to (M_1, M_4) or (M_2, M_3), the current difference i_C $(= i_L - i_p)$ will charge capacitor C_C, and then, raise i_p up to i_L. The clamp branch is mainly used to limit the transient voltage imposed on the current-fed side switches. Moreover, the flyback converter can be controlled to charge the high-voltage-side capacitor to avoid over current. The clamp branch and the flyback snubber are activated during both start-up and regular boost operation modes. A nonphase-shift PWM is used to control the circuit to achieve smooth transition from start-up to regular boost operation mode.

Referring to Fig. 1, the average power P_C transferred to C_C can be determined as follows:

$$P_C = \frac{1}{2} C_C [(i_L Z_o)^2 + 2 i_L Z_o V_{C(R)}] f_s \tag{1}$$

where

$$Z_o = \sqrt{\frac{L_{\rm eq}}{C_C}}$$

$$L_{\rm eq} = L_{ll} + L_{lh} \frac{N_P^2}{N_S^2}$$

$V_{C(R)}$ stands for a regulated V_C voltage, which is close to (V_{HV} (N_P/N_S)), f_s is the switching frequency, and $L_m \gg L_{\rm eq}$. Power P_C will be transferred to the high-side voltage source through the flyback snubber, and the snubber will regulate clamping-capacitor voltage V_C to $V_{C(R)}$ within one switching cycle T_s $(=1/f_s)$. Note that the flyback snubber does not operate over the interval of inductance current i_p increasing toward i_L. The processed power P_C by the flyback snubber is typically around 5% of the full-load power for low-voltage applications. With the flyback snubber, the energy absorbed in C_C will not flow through switches M_1–M_4, which can reduce their current stress dramatically when $L_{\rm eq}$ is significant. Theoretically, it can reduce the current stress from $2i_L$ to i_L.

The peak voltage $V_{C(P)}$ of V_C will impose on M_1–M_4 and it can be determined as follows:

$$V_{C(P)} = i_{L(M)} Z_o + V_{HV} \frac{N_p}{N_s} \tag{2}$$

where $i_{L(M)}$ is the maximum inductor current of i_L, which is related to the maximum load condition. Additionally, for reducing conduction loss, the high-side switches M_5–M_8 are operated with synchronous switching. Reliable operation and high efficiency of the proposed converter are verified on a prototype designed for alternative energy applications.

The operation waveforms of step-up conversion are shown in Fig. 2. A detailed description of a half-switching cycle operation is shown as follows.

Mode 1 [$t_0 \le t < t_1$]: In this mode, all of the four switches M_1–M_4 are turned ON. Inductor L_m is charged by V_{LV}, inductor current i_L increases linearly at a slope of V_{LV}/L_m, and the primary winding of the transformer is short-circuited. The equivalent circuit is shown in Fig. 3(a).

Mode 2 [$t_1 \le t < t_2$]: At t_1, M_1 and M_4 remain conducting, while M_2 and M_3 are turned OFF. Clamping diode D_c conducts until the current difference $(i_L(t_2) - i_p(t_2))$ drops to zero at $t = t_2$. Moreover, the body diodes of switch pair (M_5, M_8) are conducting to transfer power. During this interval, the current difference $(i_L(t) - i_p(t))$ flows into clamping capacitor C_C. The equivalent circuit is shown in Fig. 3(b).

Mode 3 [$t_2 \le t < t_3$]: At t_2, clamping diode D_c stops conducting, and the flyback snubber starts to operate. At this time, clamping capacitor C_c is discharging, and flyback inductor is storing energy. Switches M_1 and M_4 still stay in the ON state, while M_2 and M_3 remain OFF. The body diodes of switch pair (M_5, M_8) remain ON to transfer power. The equivalent circuit is shown in Fig. 3(c).

Mode 4 [$t_3 \le t < t_4$]: At t_3, the energy stored in flyback inductor is transferred to the high-voltage side. Over this interval, the flyback snubber will operate independently to regulate V_C to $V_{C(R)}$. On the other hand, switches M_1 and M_4 and diodes D_5

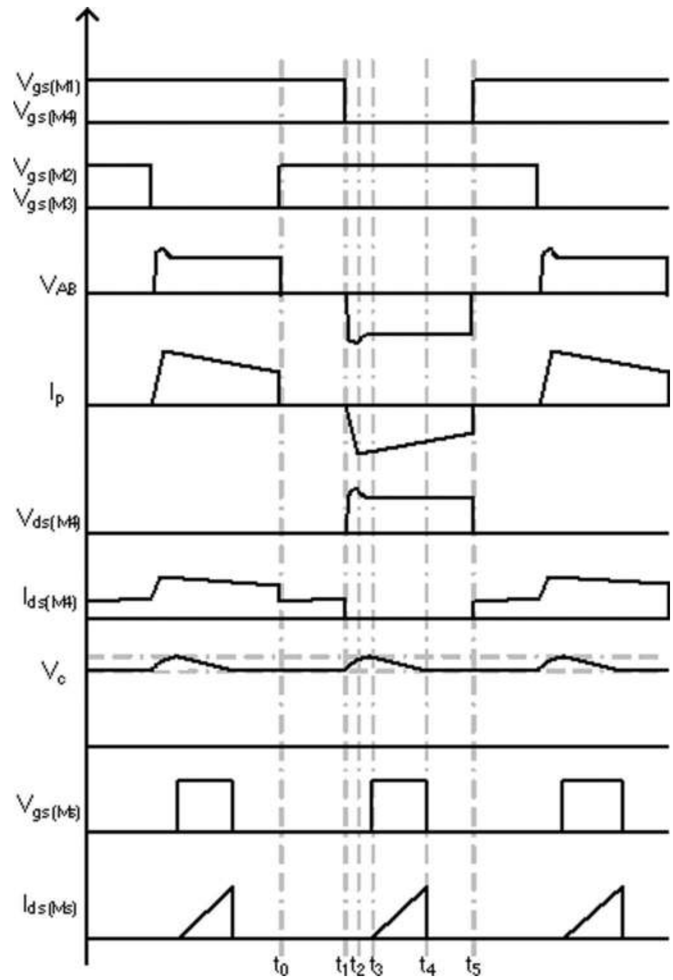

Fig. 2. Operation waveforms of step-up conversion.

and D_8 are still conducting to transfer power from V_{LV} to V_{HV}. The equivalent circuit is shown in Fig. 3(d).

Mode 5 [$t_4 \leq t < t_5$]: At t_4, capacitor voltage V_C has been regulated to $V_{C(R)}$, and the snubber is idle. Over this interval, the main power stage is still transferring power from V_{LV} to V_{HV}. It stops at t_5 and completes a half-switching cycle operation. The equivalent circuit is shown in Fig. 3(e).

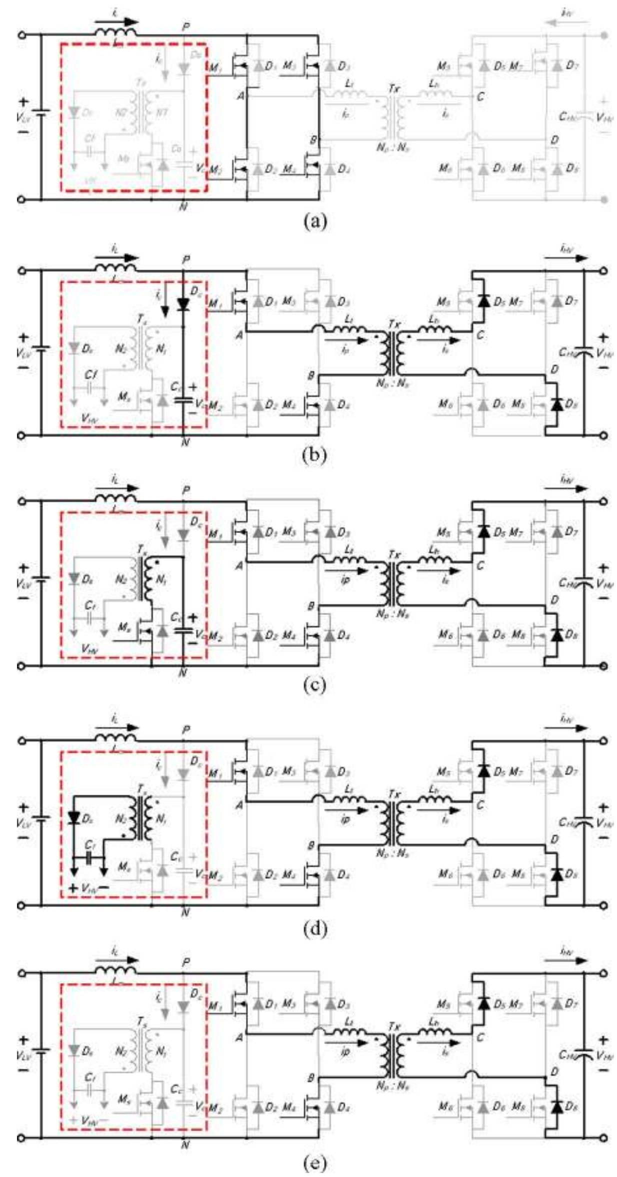

Fig. 3. Operation modes of step-up conversion. (a) Mode 1. (b) Mode 2. (c) Mode 3. (d) Mode 4. (e) Mode 5.

B. Step-Down Conversion

In the analysis, leakage inductance of the transformer at the low-voltage side is reflected to the high-voltage side, as shown in Fig. 4, in which equivalent inductance $L^*_{\rm eq}$ equals $(L_{lh} + L_{ll}(N_p^2/N_s^2))$. This circuit is known as a phase-shift full-bridge converter. In the step-down conversion, switches M_5–M_8 are operated like a buck converter, in which switch pairs (M_5, M_8) and (M_6, M_7) are alternately turned ON to transfer power from V_{HV} to V_{LV}. Switches M_1–M_4 are operated with synchronous switching to reduce conduction loss. For alleviating leakage inductance effect on voltage spike, switches M_5–M_8 are operated with phase-shift manner. Although, there is no need to absorb the current difference between i_L and i_p, capacitor C_C can help to clamp the voltage ringing due to $L_{\rm eq}$ equals $(L_{ll} + L_{lh}(N_p^2/N_s^2))$ and parasitic capacitance of M_1–M_4.

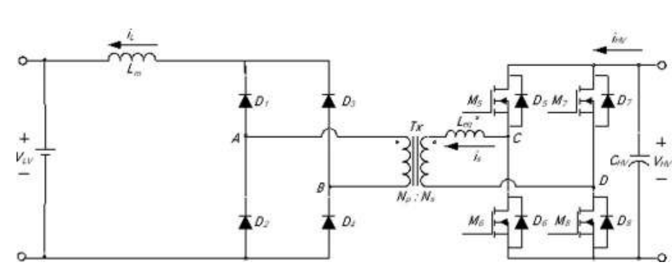

Fig. 4. Phase-shift full-bridge converter topology.

The operation waveforms of step-down conversion are shown in Fig. 5. A detailed description of a half-switching cycle operation is shown as follows.

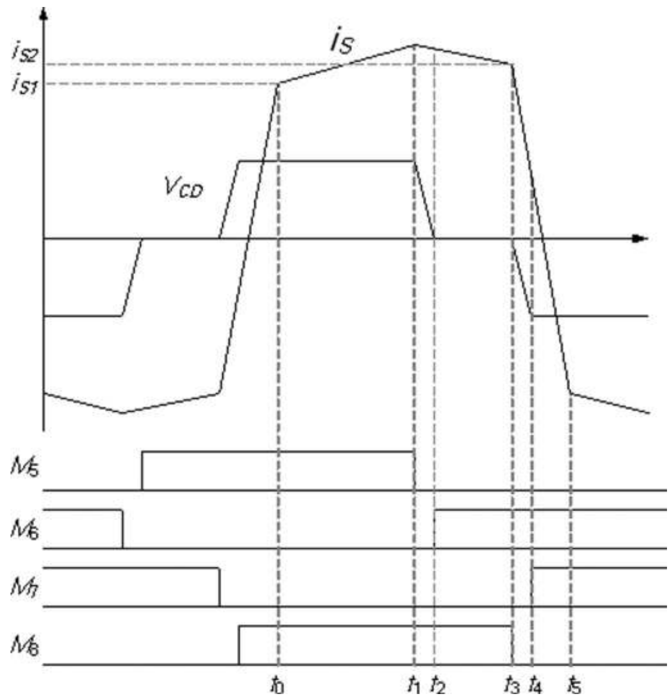

Fig. 5. Operation waveforms of step-down conversion.

Mode 1 [$t_0 \le t < t_1$]: In this mode, M_5 and M_8 are turned ON, while M_6 and M_7 are in the OFF state. The high-side voltage V_{HV} is immediately exerted on the transformer, and the whole voltage, in fact, is exerted on the equivalent inductance $L^*_{\rm eq}$ and causes the current to rise with the slope of $V_{HV}/L^*_{\rm eq}$. With the transformer current increasing linearly toward the load current level at t_1, the switch pair (M_1, M_4) are conducting to transfer power, and the voltage across the transformer terminals on the current-fed side changes immediately to reflect the voltage from the voltage-fed side, i.e., (V_{HV} (N_p/N_s)). The equivalent circuit is shown in Fig. 6(a).

Mode 2 [$t_1 \le t < t_2$]: At t_1, M_8 remains conducting, while M_5 is turned OFF. The body diode of M_6 then starts to conduct the freewheeling leakage current. The transformer current reaches the load-current level at t_1, and V_{AB} rise to the reflected voltage ($V_{HV}(N_p/N_s)$). Clamping diode D_c starts to conduct the resonant current of $L_{\rm eq}$ and the clamp capacitor C_C. This process ends at t_2 when the resonance goes through a half resonant cycle and is blocked by the clamping diode D_c. The equivalent circuit is shown in Fig. 6(b).

Mode 3 [$t_2 \le t < t_3$]: At t_2, with the body diode of switch M_6 conducting, M_6 can be turned ON with zero-voltage switching (ZVS). The equivalent circuit is shown in Fig. 6(c).

Mode 4 [$t_3 \le t < t_4$]: At t_3, M_6 remains conducting, while M_8 is turned OFF. The body diode of M_7 then starts to conduct the freewheeling leakage current. The equivalent circuit is shown in Fig. 6(d).

Mode 5 [$t_4 \le t < t_5$]: At t_4, with the body diode of switch M_7 conducting, M_7 can be turned ON with ZVS. Over this interval, the active switches change to the other pair of diagonal switches, and the voltage on the transformer reverses its polarity

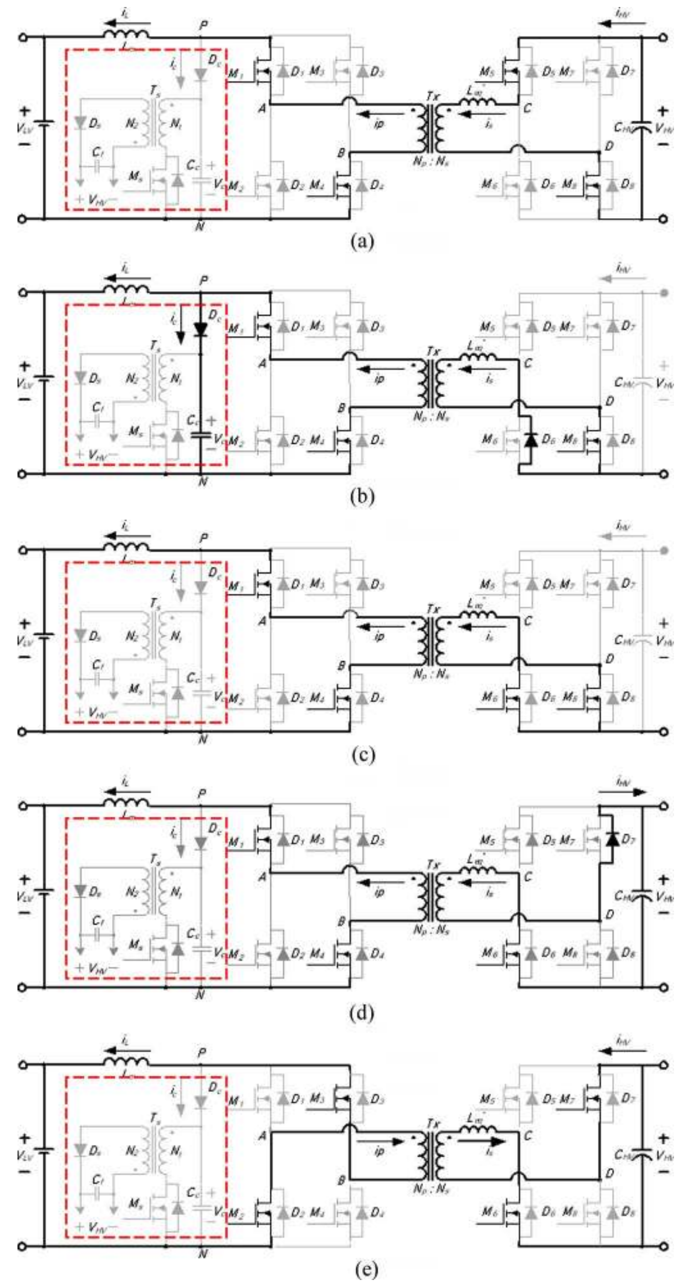

Fig. 6. Operation modes of step-down conversion. (a) Mode 1. (b) Mode 2. (c) Mode 3. (d) Mode 4. (e) Mode 5.

to balance flux. It stops at t_5 and completes a half-switching cycle operation. The equivalent circuit is shown in Fig. 6(e).

III. Practical Consideration

A. Low-Voltage Side

Switch pairs (M_1, M_4) and (M_2, M_3) are turned ON alternately under any load condition. Its minimum conduction time is

$$T_{C(\min)} = \frac{L_{\rm eq} i_L}{V_{AB}}. \quad (3)$$

B. Clamping Capacitor

For absorbing the energy stored in the leakage inductance and to limit the capacitor voltage to a specified minimal value $V_{c,l}$, capacitance C_c has to satisfy the following inequality:

$$C_c \geq \frac{L_{\text{eq}}(i_L - i_P)^2}{V_{C,l}^2}. \tag{4}$$

C. Flyback Converter

In the interval of $t_1 \leq t \leq t_2$, the high transient voltage occurs inevitably in boost mode, which could be suppressed by the clamp branch (D_c, C_c). The energy stored in capacitor C_c is transferred to the high-voltage side via a flyback converter. The regulated voltage level of the flyback converter is set between 110%–120% of the steady-state voltage at the low-voltage side. Power rating of the flyback converter can be expressed as follows:

$$P_{FB} = 0.5C_c(V_{c,h}^2 - V_{c,l}^2)f_s \tag{5}$$

where $V_{c,h}$ is the maximum voltage of V_c, $V_{c,l}$ is the minimum voltage of V_c, and f_s is the switching frequency.

D. Start-Up Operation

High inrush current with the isolated boost converter is the start-up problem before the high-side voltage is established. The initial high-side voltage V_{HV} should not be lower than $V_{LV}(N_S/N_P)$ to avoid inrush current. The proposed flyback snubber can be controlled to precharge the high-side capacitor. The operation principle is very similar to the active clamp flyback converter. Before the boost mode, the flyback converter starts to operate. Since the power rating of the flyback snubber is much lower than that of the main power stage, inductor L_m is operated in discontinuous condition mode. The start-up process usually lasts for a short period.

IV. Experimental Results

For comparison, three prototypes, the dual full-bridge converters with an *RCD* passive snubber, an active clamping circuit, and the proposed flyback snubber, were built and tested. The one with an *RCD* passive snubber is shown in Fig. 7, and Fig. 8 shows prototype with an active clamping circuit. A block diagram of the isolated bidirectional full-bridge dc–dc converter with the proposed flyback snubber is shown in Fig. 9, describing the signal flow and linkage between the power stage and the controller. It was implemented with the specifications listed in Table I, and the circuit diagram shown in Fig. 1. Note that the picture of a 1.5-kW experimental prototype with the proposed configuration is shown in Fig. 10. A battery module working at the low-voltage side is employed as an energy-storage element, whose voltage rating is 48 V. The high-voltage side is 360 V.

Equations (1), (2), and (5) show that inductor current i_L and clamping capacitor C_C can all influence the processed power P_C and excess voltage V_E $(= V_{C(P)} - V_{PL})$ in the proposed converter. Impacts of different control parameters to the performance of the proposed converter are verified with computer

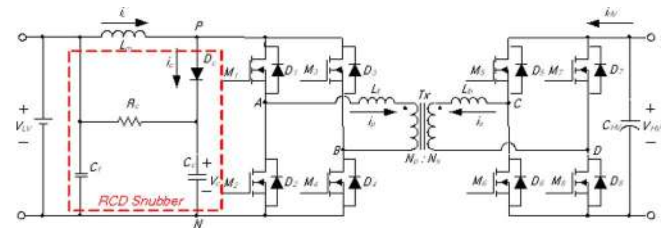

Fig. 7. Isolated bidirectional full-bridge dc–dc converter with an *RCD* passive snubber.

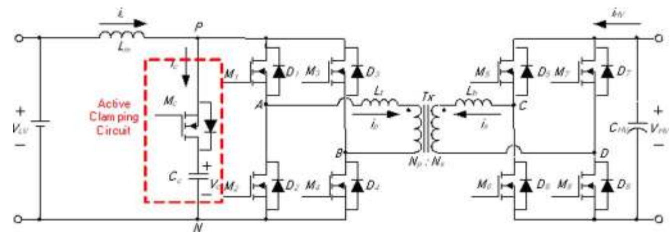

Fig. 8. Isolated bidirectional full-bridge dc–dc converter with an active clamping circuit.

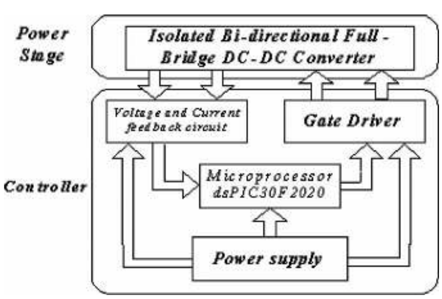

Fig. 9. Block diagram of the isolated bidirectional full-bridge dc–dc converter with the proposed flyback snubber.

TABLE I
Specifications of the Prototype

Low-side Voltage	V_{LV} = 48 V
High-side Voltage	V_{HV} = 360 V
Output Power	$P_{o(max)}$ = 1.5 kW
Switching Frequency	f_s = 25 kHz
Turns Ratio	$N = N_p / N_s$ = 4.26
Leakage Inductance	L_{ll} = 0.5 μH, L_{lh} = 9 μH
Current-fed Inductor	L_m = 500 μH
Clamping Capacitor	C_C = 1 μF
Low-side Switches	$M_1 \sim M_4$: IRFB4321PbF (150V/83A) ×2
Low-side Capacitor	C_{LV} : 100 μF
Low-side Inductor	L_m : 500 μH
High-side Switches	$M_5 \sim M_8$: IRFP26N60LPBF (600V/26A)
High-side Capacitor	C_{HV} : 470μF×2

Fig. 10. Photograph of the prototype converter.

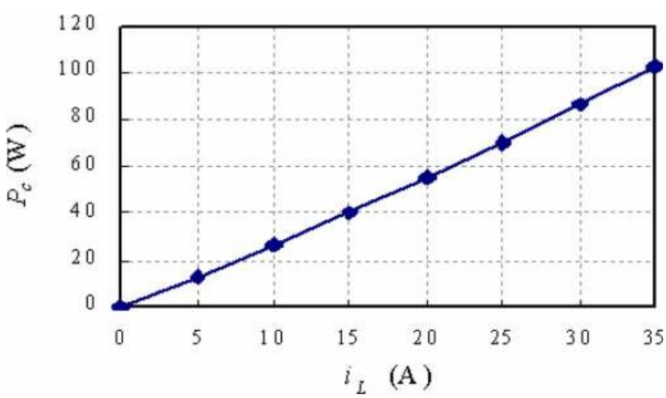

Fig. 11. Plot of the processed power P_C versus inductor current i_L (C_C = 1 μF, $L_{\rm eq}$ = 1 μH, and Z_O = 1 Ω).

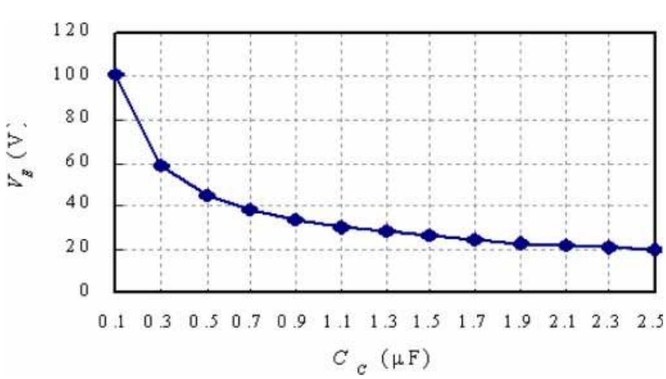

Fig. 12. Plot of excess voltage V_E (= $V_{C(P)} - V_{PL}$) versus clamping capacitor C_C (i_L = 32 A, V_{PL} = 85 V, and $L_{\rm eq}$ = 1 μH), where $V_{\rm PL} \approx V_{C(R)}$.

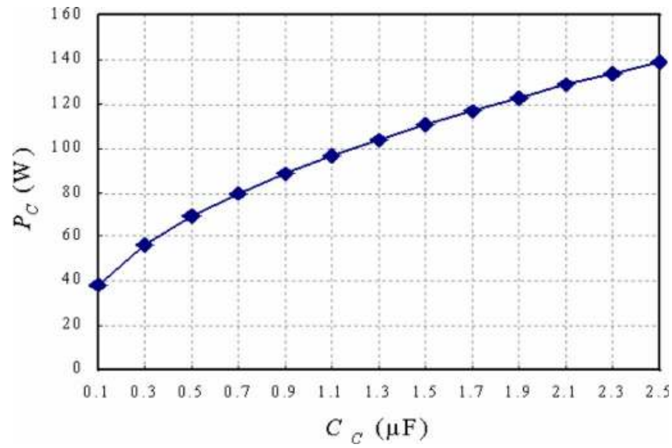

Fig. 13. Plot of the processed power P_C versus clamping capacitor C_C (i_L = 32 A and $L_{\rm eq}$ = 1 μH).

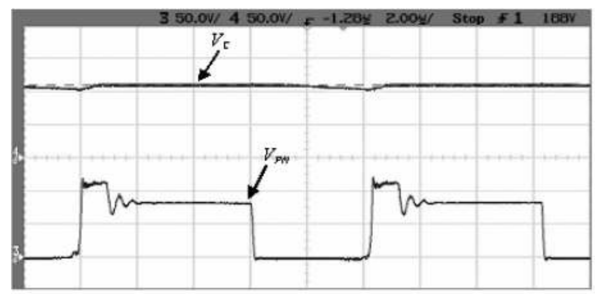

(V_C : 50 V/div, V_{PN} : 50 V/div, Time : 2 μs/div)

Fig. 14. Measured voltage waveforms of V_C and V_{PN} from high-voltage to low-voltage conversion (360 V → 48 V).

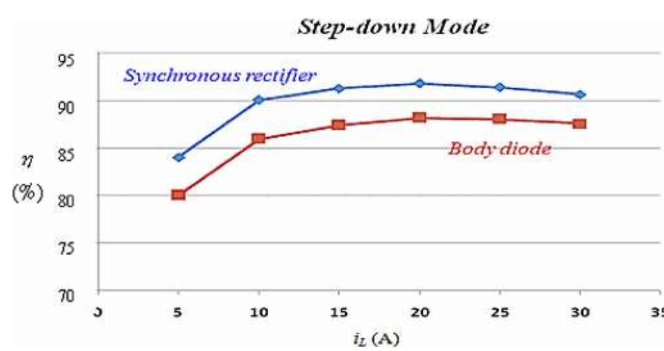

Fig. 15. Plots of conversion efficiency of the bidirectional converter operated in step-down mode.

simulation results. Fig. 11 shows plot of the processed power P_C versus i_L, which reveals that the maximum P_C under 1.5 kW is around 90 W. Fig. 12 shows a plot of voltage ($V_{C(P)} - V_{PL}$) versus C_C when $L_{\rm eq}$ is fixed, from which it can be seen that an increment of C_C will result not only in low $V_{C(P)}$, but also result in high P_C, as shown in Fig. 13.

Voltage waveforms of V_c and V_{PN} from high-voltage to low-voltage conversion (360 V → 48 V) are shown in Fig. 14. It can be found that the proposed converter has a significant reduction of voltage spike in step-down conversion operation.

Fig. 15 shows plots of conversion efficiency of the bidirectional converter operated in step-down mode. It can be observed that when the circuit is operated under heavy-load condition, high conduction loss will result in lower conversion efficiency. Furthermore, using synchronous switching can yield higher conversion efficiency than that with the body diodes.

Fig. 16 shows measured waveforms of primary-side current I_P and voltage V_{PN} during step-up conversion from the converter with an *RCD* passive snubber. It can be seen that low

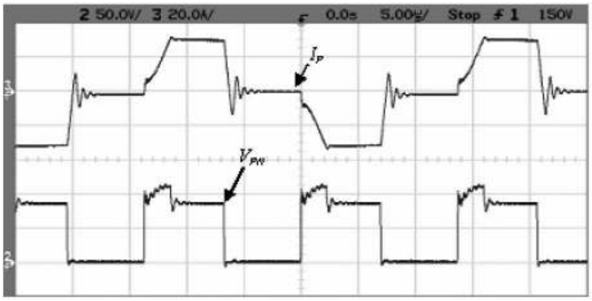

(I_P : 20 A/div, V_{PN} : 50 V/div, Time : 5 µs/div)

Fig. 16. Measured waveforms of I_P and V_{PN} from low-voltage to high-voltage conversion (48 V → 360 V) with a *RCD* passive snubber.

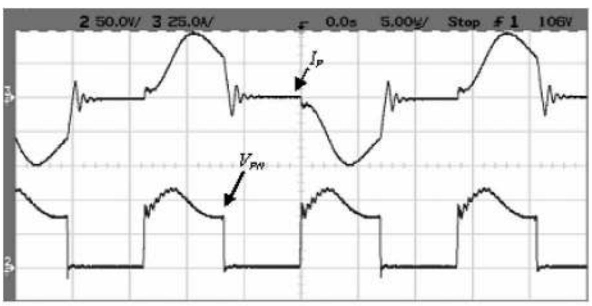

(I_P : 25 A/div, V_{PN} : 50 V/div, Time : 5 µs/div)

Fig. 17. Measured waveforms of I_P and V_{PN} from low-voltage to high-voltage conversion (48 V → 360 V) with an active clamping circuit.

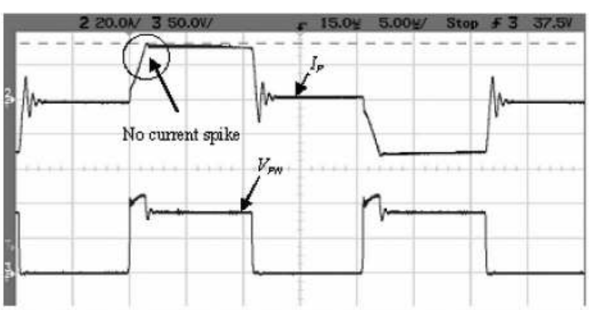

(I_P : 20 A/div, V_{PN} : 50 V/div, Time : 5 µs/div)

Fig. 18. Measured waveforms of I_P and V_{PN} from low-voltage to high-voltage conversion (48 V → 360 V) with the flyback snubber.

current and voltage stress can be achieved. However, since the average power dissipation on resistor R_C under the full-load condition is about 107.46 W, its conversion efficiency is only about 82%. Fig. 17 shows those waveforms with an active clamping circuit, and the waveform shows that high peak current (48.1 A) has been observed. Conversion efficiency of the converter under the full-load condition and with an active clamping circuit is about 87.2%. Fig. 18 shows those with the proposed flyback snubber. It can be found that the flyback snubber can absorb the current difference between the current-fed inductor and leakage inductance of the isolation transformer; therefore, voltage spikes of the switches can be reduced. Moreover, since the snubber current does not circulate through the low-side switches, their peak current has been well suppressed. Conversion efficiency of the

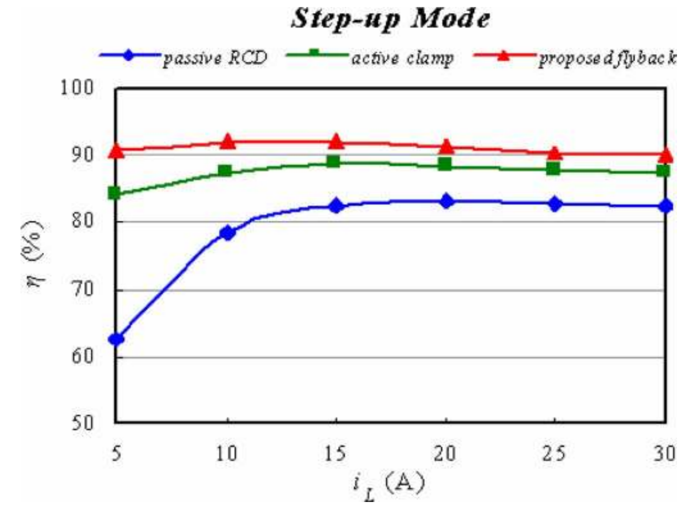

Fig. 19. Plots of conversion efficiency of the bidirectional converter with various snubber operated in step-up mode.

converter under the full-load condition and with the proposed snubber is about 90%.

Fig. 19 shows plot of conversion efficiency of the bidirectional converter with various snubbers operated in step-up mode. It can be observed that the conversion efficiency of the proposed converter is around 90%–92%, which is higher than the other two types.

V. Conclusion

This paper has presented an isolated bidirectional full-bridge dc–dc converter with a flyback snubber for high-power applications. The flyback snubber can alleviate the voltage spike caused by the current difference between the current-fed inductor and leakage inductance of the isolation transformer, and can reduce the current flowing through the active switches at the current-fed side by 50%. Since the current does not circulate through the full-bridge switches, their current stresses can be reduced dramatically under heavy-load condition, thus improving system reliability significantly. The flyback snubber can be also controlled to achieve a soft start-up feature. It has been successful in suppressing inrush current which is usually found in a boost-mode start-up transition. A 1.5-kW isolated full-bridge bidirectional dc–dc converter with a flyback snubber has been implemented to verify its feasibility.

References

[1] H. Bai and C. Mi, “Eliminate reactive power and increase system efficiency of isolated bidirectional dual-active-bridge DC-DC converters using novel dual-phase-shift control,” *IEEE Trans. Power Electron.*, vol. 23, no. 6, pp. 2905–2914, Dec. 2008.

[2] B. Bai, C. Mi, and S. Gargies, “The short-time-scale transient processes in high-voltage and high-power isolated bidirectional DC-DC converters,” *IEEE Trans. Power Electron.*, vol. 23, no. 6, pp. 2648–2656, Nov. 2008.

[3] C. Zhao, S. D. Round, and J. W. Kolar, “An isolated three-port bidirectional DC-DC converter with decoupled power flow management,” *IEEE Trans. Power Electron.*, vol. 23, no. 5, pp. 2443–2453, Sep. 2008.

[4] R. Huang and S. K. Mazumder, “A soft-switching scheme for an isolated DC/DC converter with pulsating DC output for a three-phase high-frequency-link PWM converter,” *IEEE Trans. Power Electron.*, vol. 24, no. 10, pp. 2276–2288, Oct. 2009.

[5] H. Xiao and S. Xie, "A ZVS bidirectional dc-dc converter with phased-shift plus PWM control scheme," *IEEE Trans. Power Electron.*, vol. 23, no. 2, pp. 813–823, Mar. 2008.

[6] G. Ma, W. Qu, and Y. Liu, "A zero-voltage-switching bidirectional DC-DC converter with state analysis and soft-switching-oriented design consideration," *IEEE Trans. Ind. Electron.*, vol. 56, no. 6, pp. 2174–2184, Jun. 2009.

[7] F. Krismer and J. W. Kolar, "Accurate small-signal model for the digital control of an automotive bidirectional dual active bridge," *IEEE Trans. Power Electron.*, vol. 24, no. 12, pp. 2756–2768, Dec. 2009.

[8] F. Barone, "A lightweight inverter for off-grid and grid-connected systems," in *Proc. Photovoltaic Spec. Conf.*, 1994, vol. 1, pp. 917–920.

[9] T. Reimann, S. Szeponik, and G. Berger, "A novel control principle of bi-directional DC-DC power conversion," in *Proc. Power Electron. Spec. Conf.*, 1997, vol. 2, pp. 978–984.

[10] K. Wang, C. Y. Lin, L. Zhu, D. Qu, F. C. Lee, and J. S. Lai, "Bi-directional DC to DC converters for fuel cell systems," in *Proc. Power Electron. Transp.*, 1998, pp. 47–51.

[11] H. L. Chan, K. W. E. Cheng, and D. Sutanto, "A phase-shift controlled bi-directional DC-DC converter," in *Proc. Circuits Syst.*, 1999, vol. 2, pp. 723–726.

[12] S. Yujin and P. N. Enjeti, "A new soft switching technique for bi-directional power flow, full-bridge DC-DC converter," in *Proc. Ind. Appl. Conf.*, 2002, vol. 4, pp. 2314–2319.

[13] O. Garcia, L. A. Flores, J. A. Oliver, J. A. Cobos, and J. De la pena, "Bi-directional DC-DC converter for hybrid vehicles," in *Proc. Power Electron. Spec. Conf.*, 2005, pp. 1881–1886.

[14] L. Zhu, "A novel soft-commutating isolated boost full-bridge ZVS-PWM DC-DC converter for bidirectional high power applications," *IEEE Trans. Power Electron.*, vol. 21, no. 2, pp. 422–429, Mar. 2006.

[15] H. Krishnaswami and N. Mohan, "A current-fed three-port bi-directional DC-DC converter," in *Proc. Telecommun. Energy Conf.*, 2007, pp. 523–526.

[16] D. Aggeler, J. Biela, S. Inoue, H. Akagi, and J. W. Kolar, "Bi-directional isolated DC-DC converter for next-generation power distribution comparison of converters using Si and SiC devices," in *Proc. Power Convers. Conf.*, 2007, pp. 510–517.

[17] C. Qiao and K. M. Smedley, "An isolated full bridge boost converter with active soft switching," in *Proc. Power Electron. Spec. Conf.*, 2001, pp. 896–903.

[18] L. Zhou and X. Ruan, "A zero-current and zero-voltage-switching PWM boost full-bridge converter," in *Proc. Power Electron. Spec. Conf.*, 2003, pp. 957–962.

[19] R. Watson and F. C. Lee, "A soft-switched, full-bridge boost converter employing an active-clamp circuit," in *Proc. Power Electron. Spec. Conf.*, 1996, pp. 1948–1954.

[20] K. Wang, F. C. Lee, and J. Lai, "Operation principles of bi-directional full-bridge DC/DC converter with unified soft-switching scheme and soft-starting capability," in *Proc. Appl. Power Electron. Conf.*, 2000, pp. 111–118.

Tsai-Fu Wu (S'88–M'91–SM'97) received the B.S. degree in electronic engineering from the National Chiao-Tung University, Hsinchu, Taiwan, in 1983, the M.S. degree in electrical and computer engineering from Ohio University, Athens, in 1988, and the Ph.D. degree in electrical engineering and computer science from the University of Illinois, Chicago, in 1992.

From 1985 to 1986, he was a System Engineer at SAMPO, Inc., Taiwan, where he was engaged in developing and designing graphic terminals. From 1988 to 1992, he was a Teaching and a Research Assistant in the Department of Electrical Engineering and Computer Science, University of Illinois. Since 1993, he has been in the Department of Electrical Engineering, National Chung Cheng University, Min-Hsiung, Taiwan, where he is currently a Chair Professor and the Director of the Elegant Power Application Research Center. His research interests include developing and modeling of power converters, design of electronic dimming ballasts for fluorescent lamps, metal halide lamps and plasma display panels, design of solar-array supplied inverters for grid connection, and design of pulsed-electrical-field generators for transdermal drug delivery and food pasteurization.

Prof. Wu is a Senior Member of the Chinese Institute of Engineers. He was the recipient of the three Best Paper Awards from Taipei Power Electronics Association in 2003–2005. In 2006, he was awarded as an Outstanding Researcher by the National Science Council, Taiwan.

Yung-Chu Chen received the B.S. degree in electronic engineering from Taiwan Institute of Technology, Taipei, Taiwan, in 1993, the M.S. degree in electrical engineering from the National Chung Cheng University, Min-Hsiung, Taiwan, in 2002, from where he is currently working toward the Ph.D. degree from the Elegant Power Application Research Center, Department of Electrical Engineering.

His current research interests include design of converters and inverters and renewable energy systems.

Jeng-Gung Yang was born in Taiwan, in 1985. He received the B.S. degree in electrical engineering from the National Chung Cheng University, Min-Hsiung, Taiwan, in 2009, where he is currently working toward the M.S. degree.

His current research interests include design and development of soft switching power converters.

Chia-Ling Kuo was born in Taiwan, in 1985. She received the B.S. degree in electrical engineering from the National Chung Cheng University, Min-Hsiung, Taiwan, in 2009, where she is currently working toward the M.S. degree.

Her current research interests include design and implementation of bidirectional inverters.